Materials Science-Poland, 33(4), 2015, pp. 852-861
http://www.materialsscience.pwr.wroc.pl/
DOI: 10.1515/msp-2015-0107

DE GRUYTER OPEN

Structural and electrical properties of barium titanate ($BaTiO_3$) thin films obtained by spray pyrolysis method

S.S. KUMBHAR, M.A. MAHADIK, P.K. CHOUGULE, V.S. MOHITE, Y.M. HUNGE, K.Y. RAJPURE, A.V. MOHOLKAR, C.H. BHOSALE*

Electrochemical Materials Laboratory, Department of Physics, Shivaji University, Kolhapur 416004, India

Barium titanate ($BaTiO_3$) thin films have been prepared using the spray pyrolysis method. The films were deposited onto a glass substrate at varying substrate temperature ranging from 250 to 350 °C with the interval of 50 °C. The structural, morphological, electrical and dielectric properties of the deposited films have been studied. The X-ray diffraction pattern confirmed the polycrystalline nature of the films with a cubic crystal structure. X-ray photoelectron spectroscopy (XPS) showed a good agreement of the thin films stoichiometry with $BaTiO_3$. A presence of Ba, Ti and O in the $BaTiO_3$ thin films was observed by energy dispersive X-ray analysis. The scanning electron microscopy (SEM) showed the heterogeneous distribution of cubical grains all over the substrate. The grain size decreased with an increase in substrate temperature. The dielectric constant and dielectric loss showed the dispersion behaviour as a function of frequency, measured in the frequency range of 20 Hz to 1 MHz. The AC conductivity (σ_{ac}) measurement showed the linear nature of obtained films, which confirms conduction mechanism due to small polarons. Impedance spectroscopy has been used to study the electrical behaviour of $BaTiO_3$ ferroelectric thin films. The ferroelectric hysteresis loop has been recorded at room temperature.

Keywords: *$BaTiO_3$ thin films; structural properties; dielectric properties*

1. Introduction

In recent years, $BaTiO_3$ thin films have been one of the most promising material because of its ferroelectricity, high dielectric constant and large electro-optic coefficients, which attracted considerable attention of many researchers. This has been motivated by its low dissipation factor, low leakage current and high breakdown field. Like in other electronic ceramic materials, the electrical properties of $BaTiO_3$ are closely linked to its microstructural features, such as porosity and grain size. For optimal properties it is desirable to have a homogeneous microstructure for optimal properties. In principle, $BaTiO_3$ ceramics with a dense structure and fine grains has very good dielectric properties. The $BaTiO_3$ thin films with perovskite structure are of particular interest for electronic device applications due to their useful ferroelectric properties [1–3]. Many attempts have been tried to integrate the ferroelectric thin films of $BaTiO_3$ to design non-volatile memory devices and integrated transducers [4, 5]. Initially, various research groups have been working on the bulk form of $BaTiO_3$ but nowadays, due to downsizing and miniaturization of integrated circuits, there are more and more demands imposed on the thin films of $BaTiO_3$ technological applications [6]. The thin films of $BaTiO_3$ also possess piezoelectricity as well as optical and dielectric properties [7]. Thus, the thin films of $BaTiO_3$ are useful for dynamic random access memories (DRAMS), electro-optic switches, thin film capacitors and modulators [8]. These thin films may be applied in the next-generation FRAM and DRAM technologies and to advanced optical devices [9]. Normally, a ferroelectric capacitor is made from a layer of ferroelectric material sandwiched in a pair of electrodes. The spontaneous polarization effect in ferroelectric material implies a hysteresis phenomenon, which can be used as a memory function and ferroelectric capacitors. The $BaTiO_3$ thin films can be prepared by various

*E-mail: chbhosale@gmail.com

deposition methods, such as chemical route [10], ion beam deposition [11], pulse laser deposition (PLD) [12], sol-gel [13], RF-magnetron sputtering [14], microwave hydrothermal process [15], etc. In comparison with other deposition techniques, spray pyrolysis has several advantages, such as high purity, excellent control of chemical uniformity and stoichiometry in multi-component systems. The other advantage of the spray pyrolysis method is that it can be adapted easily for production of large-area thin films. The spray pyrolysis method is widely used to grow complex, multilayered thin films because of its ability to preserve the target stoichiometry to prepare thin films by layer-by-layer growth. The spray pyrolysis method has many advantages, such as simplicity, low cost and easy adjusting of various deposition parameters to prepare thin films from various spray solutions [16]. Panda et al. [17] studied the optical properties of strontium substituted $BaTiO_3$ thin films prepared by RF-sputtering method. From this they concluded that the optical band gap decreased with an increase of Ba content in the film, achieving a typical value of 3.31 eV for $Ba_{0.8}Sr_{0.2}TiO_3$. Wang et al. [18] studied the sensing properties of $BaTiO_3$ thin films prepared by spin coating method. From this, they found out that at low frequency measurements the capacitance of the sensor increases as relative humidity (RH) increases. James et al. [19] studied the structural properties and impedance spectroscopy of Zr substituted $BaTiO_3$ thin films prepared by the laser ablation method. Qiao et al. [20] studied microstructural orientation, strain state and diffusive phase transition by pure argon sputtering method. Recently, a similar approach has been used to prepare various oxides and ferrite thin films [21]. We have successfully employed spray pyrolysis for manufacturing a number of other pure and doped thin-film compounds, such as TiO_2 [22], ZnO [23], Fe_2O_3 [24], TiO_2/ZnO [25].

In the present paper, an attempt has been made to prepare thin films of $BaTiO_3$ by using the spray pyrolysis method. The formation of nanocrystalline thin films of $BaTiO_3$ by using this method was proposed since it is promising for nanoparticle formation. The deposition temperature is low as compared to other deposition methods. Hence, the deposition of $BaTiO_3$ thin films at low temperature is an attractive feature in silicon technology [21]. The aim of this study was to understand the effects of preparation conditions on the electrical and dielectric properties of the $BaTiO_3$ thin films. The prepared films were characterized by XRD, SEM, AFM, AC conductivity, dielectric properties and impedance spectroscopy. From this study, the effect of different substrate temperatures on structural and electrical properties of the $BaTiO_3$ thin films was also studied. The prepared thin films of $BaTiO_3$ were also used for magnetoelectric (ME) composite to measure the ME voltage. The obtained results have been compared with the results of $BaTiO_3$ ferroelectric thin films prepared by other techniques. Formation of $BaTiO_3$ thin film is also very useful in technological applications.

2. Experimental

The $BaTiO_3$ thin films were prepared using the spray pyrolysis method. Barium acetate $[CH_3{\cdot}COO)_2Ba]$ (Thomas Baker, AR grade, 99.0 % purity) and titanium tetra-isopropoxide $[C_{12}H_{28}O_4Ti]$ (Spectrochem Private Limited Mumbai-India, 98 % purity) were used as starting materials. Initially, barium acetate solution was prepared by dissolving barium acetate in double distilled water. Similarly, the solution of titanium tetra-isopropoxide was prepared by dissolving titanium tetra-isopropoxide in ethanol. Finally, a spray solution was prepared by mixing these two solutions in a ratio of 1:2. The resulting 30 mL (quantity of spraying solution) solution was sprayed onto preheated glass substrates at 0.1 M concentration. The substrates were cleaned with double distilled water and then boiled in chromic acid for 1 h to remove sticky particles of oil and grease. The deposition was carried out in a temperature range of 250 to 350 °C with an interval of 50 °C. During the deposition, air was used as a carrier gas and other preparative parameters of spray, such as solution spray rate (2 $mL{\cdot}min^{-1}$), nozzle to substrate distance (32 cm) were kept constant. The structural properties of

$BaTiO_3$ thin films were studied by using Bruker D2 Phaser X-ray diffractometer with CuKα radiation. XPS spectra of $BaTiO_3$ thin films were recorded on a VG Scientific Escalab Mk I (Thermo VG Scientific, West Sussex, UK) instrument operating with a unmonochromatized AlKα X-ray source 83 (1486.6 eV). The surface morphology and EDAX spectroscopy were studied by using a JEOL JSM-6360 scanning electron microscope (SEM). Surface topography of the films was further analysed from the AFM images taken by means of an atomic force microscope (AFM, Bruker instrument, Innova 1B3BE) operated at room temperature. AFM images were collected in contact mode using a silicon nitride cantilever. The dielectric constant (ε'), loss tangent (tanδ) and impedance were measured at room temperature in the frequency range of 20 Hz to 1 MHz using LCR Meter Bridge (model HP 4284 A). PE-Hysteresis loop measurement was carried by a ferroelectric loop (P-E) tracer at room temperature.

3. Results and discussion

3.1. Structural properties

The X-ray diffraction patterns of spray deposited $BaTiO_3$ thin films are shown in Fig. 1. The X-ray diffraction patterns reveal that the films are polycrystalline in nature. The sharp and strong diffraction peaks are in agreement with those for cubic crystal structure (JCPDS Card No. 01-075-0213). There are some impurity peaks of barium carbonate ($BaCO_3$). These impurity peaks of barium carbonate ($BaCO_3$) occur because of the excess of barium oxide and thermal decomposition of barium acetate at lower temperature, and are in agreement with reported literature [26–28]. Also, Phule et al. [29] reported the presence of trace amount of $BaCO_3$ peaks in $BaTiO_3$ films obtained using barium acetate and titanium isopropoxide as starting materials. The lattice constant 'a' is calculated by the following formula:

$$d = \frac{a}{\sqrt{h^2 + k^2 + l^2}} \tag{1}$$

where (h k l) are Miller indices, 'd' is interplanar spacing and 'a' is the lattice parameter. The average value of the lattice parameter 'a' is 4.08 Å. The average crystallite size is estimated from the Scherer equation:

$$D_{hkl} = \frac{0.9\lambda}{\beta \cos\theta} \tag{2}$$

where $D_{h\,k\,l}$ is the crystallite size (nm) perpendicular to (h k l) plane, β is the full width at half maximum, θ is the Bragg angle, and λ is the wavelength of X-ray (λ = 0.15406 nm). The average crystalline size of $BaTiO_3$ films, according to the Scherrer equation, is of an order of 32 nm. The amorphous structure of the films was observed for sintering temperature of 400 °C. This may be due to the low thickness of the film.

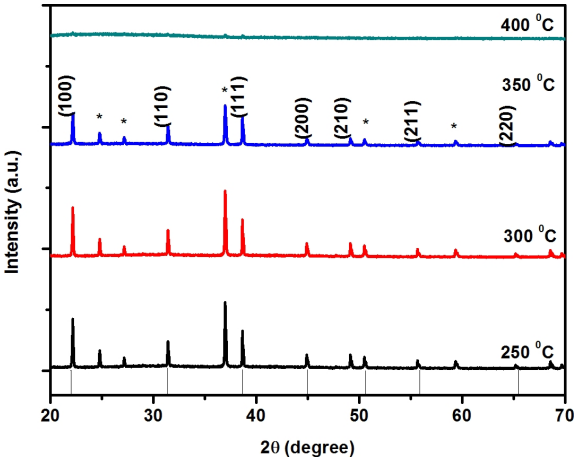

Fig. 1. X-ray diffraction patterns for $BaTiO_3$ thin films prepared at substrate temperatures of 250 to 350 °C at an interval of 50 °C.

3.2. X-ray photoelectron spectroscopy (XPS)

The survey scan spectrum of $BaTiO_3$ thin film is shown in Fig. 2a. From this survey scan spectrum it is seen that the C 1s line of the residual carbon is located at 284.77 eV. In addition to C, no other contaminant was detected on the surface of the sample. High resolution spectra of Ba3d, Ti2p and O1s photoelectron peaks were also obtained. Fig. 2b shows the narrow scan spectrum of Ba for the $BaTiO_3$ thin film. It can be seen from the XPS spectra of Ba 3d that there exists one electron state of Ba $3d_{5/2}$

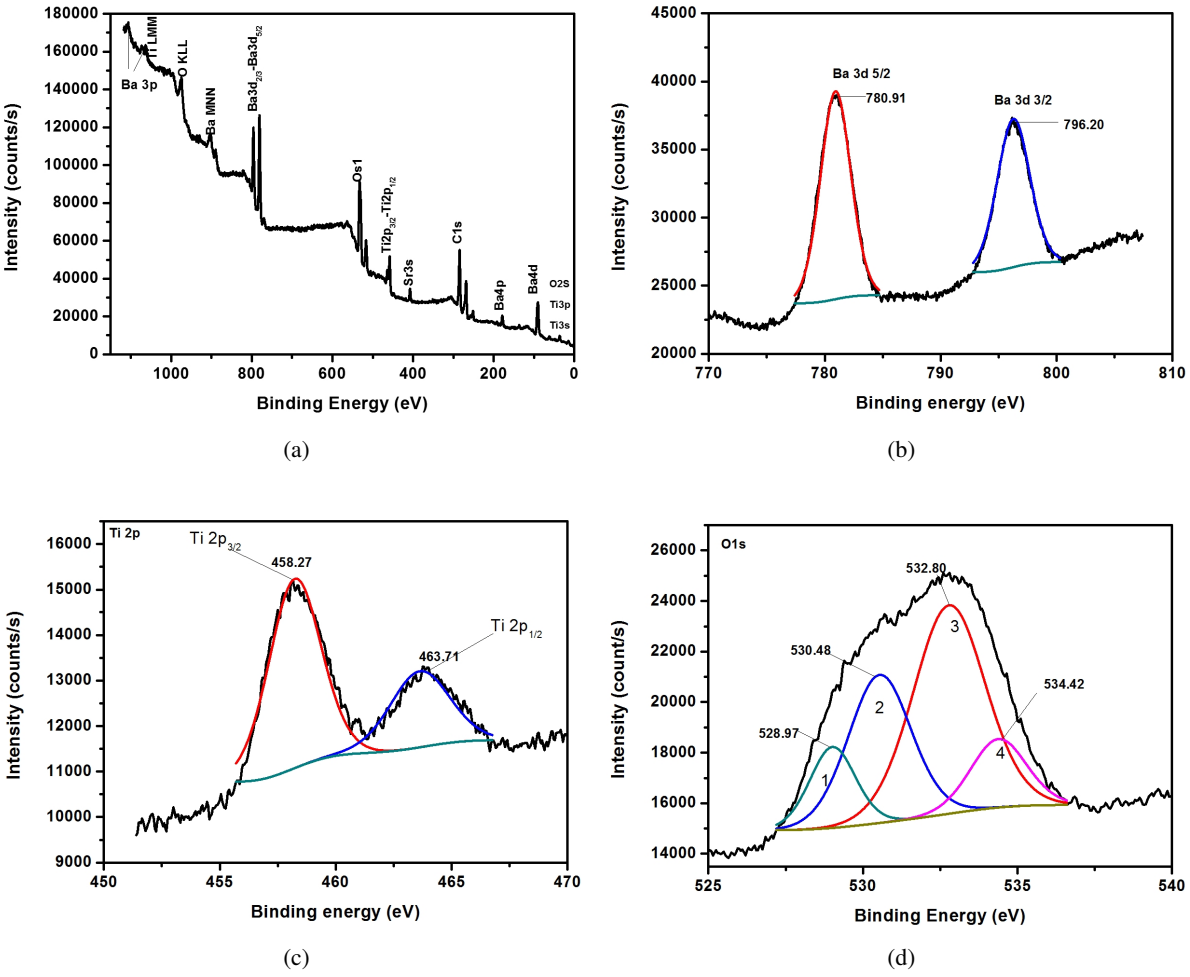

Fig. 2. (a) XPS survey scan spectrum of $BaTiO_3$ thin film; (b) Ba narrow scan spectrum of $BaTiO_3$ thin film; (c) Ti narrow scan spectrum of $BaTiO_3$ thin film; (d) O1s narrow scan spectrum of $BaTiO_3$ thin film.

in the detectable surface region with a binding energy of 779.6 eV. The Ba $3d_{5/2}$ state corresponds to the α state, which is associated with the pervoskite structure [30, 31]. The Ti narrow scan spectrum of $BaTiO_3$ thin film (Fig. 2c) shows the peaks located at 458.2 and 463.7 eV coming from $Ti2p_{3/2}$ and $Ti2p_{1/2}$. The calculated binding energies difference between $Ti2p_{3/2}$ and $Ti2p_{1/2}$ spin-orbit splitting is 5.4 eV. The spectrum of O 1s for $BaTiO_3$ thin film (Fig. 2d) shows a broad asymmetric curve which can be deconvoluted into four peaks with binding energies at 534.42, 532.80, 530.48 and 528.97 eV, respectively. The distinctive peak at 530.48 eV is assigned to the lattice oxygen in the metal oxide framework, and the peaks at 534.42, 532.80 and 528.97 eV indicate the presence of other components (such as OH, H_2O and carbonate species) adsorbed on the particle surface [31].

3.3. Energy dispersive X-ray analysis (EDAX)

Fig. 3 shows the EDAX spectra of $BaTiO_3$ thin film prepared by spray pyrolysis method at substrate temperature of 250 °C. The energy dispersive X-ray analysis indicates the presence of Ba, Ti and O in the prepared $BaTiO_3$ thin film. The concentration ratio Ba:Ti:O shows that the films are substoichiometric. The experimental values of $BaTiO_3$ thin film obtained from the spectrum of energy dispersive X-ray analysis (EDAX) are shown in Table 1.

Table 1. Experimental values of BTO thin film obtained from the spectrum of energy dispersive X-ray analysis (EDAX).

Element	Atomic %
Ba L	13.13
O K	83.73
Ti K	3.14
Total	100.00

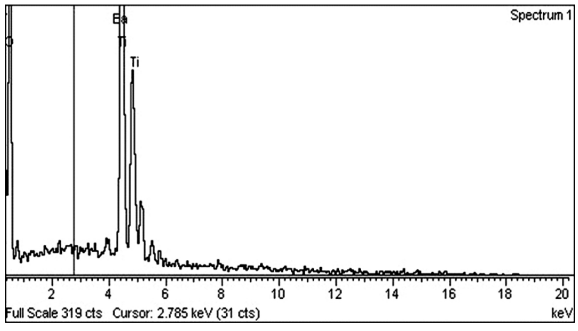

Fig. 3. EDAX spectrum of $BaTiO_3$ thin film prepared by spray pyrolysis method at substrate temperature of 250 °C.

3.4. Morphological properties

Fig. 4 shows the SEM images of $BaTiO_3$ thin films prepared at different substrate temperatures of 250 °C to 350 °C at the interval of 50 °C. The observed surface morphology shows a cube-like grain structure of the films. The SEM images depict a heterogeneous distribution of cubical grains all over the substrate. The SEM images of $BaTiO_3$ thin films show that the grain size decreases from 0.7 to 0.1 μm with an increase in substrate temperature. AFM images at higher substrate temperature depict that the films show agglomeration of grains. Fig. 5 depicts 2D and 3D AFM images of $BaTiO_3$ thin films deposited at substrate temperatures from 250 °C to 350 °C at the interval of 50 °C. From the images it is clear that the film covers the entire area of the surface with small cube-like grains, which are randomly distributed. From AFM micrographs it is also seen the grain size decreases with an increase in substrate temperature.

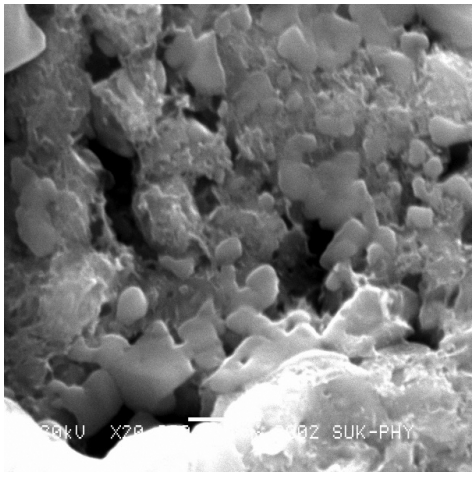

(a)

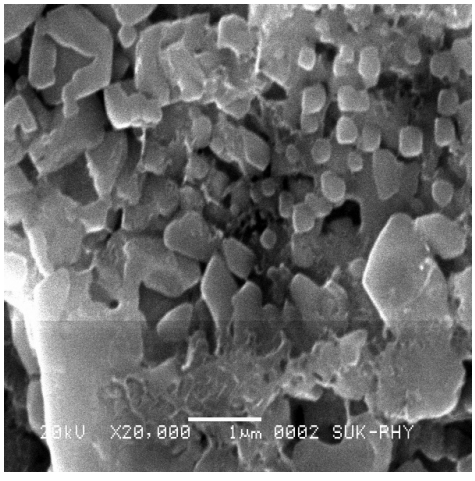

(b)

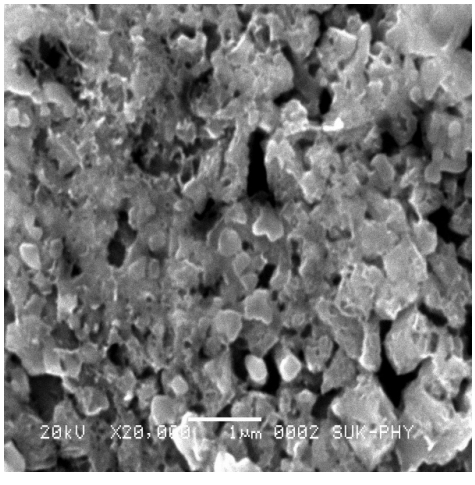

(c)

Fig. 4. SEM images of $BaTiO_3$ thin films prepared at substrate temperatures of 250 to 350 °C at an interval of 50 °C.

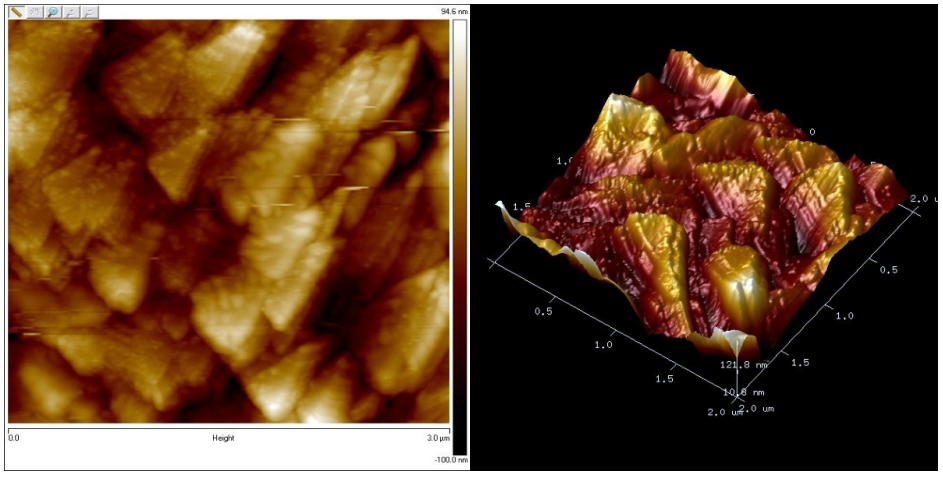

(a) (b)

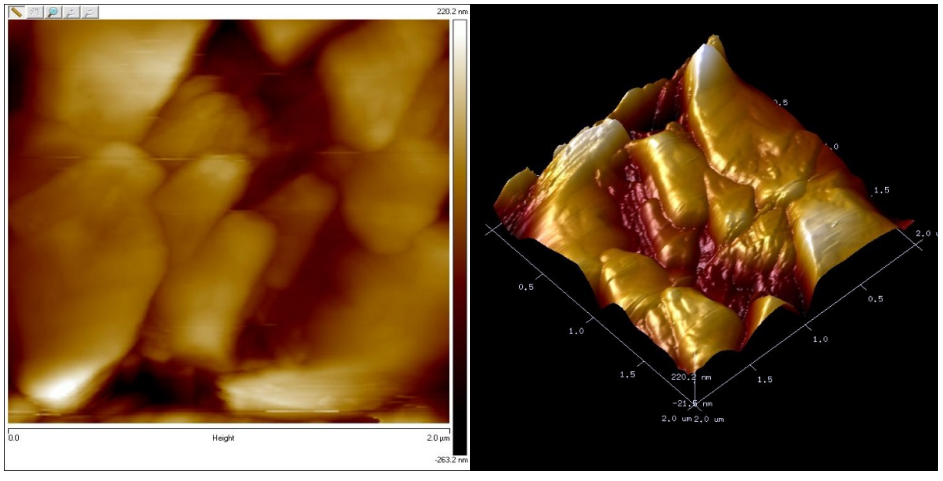

(c) (d)

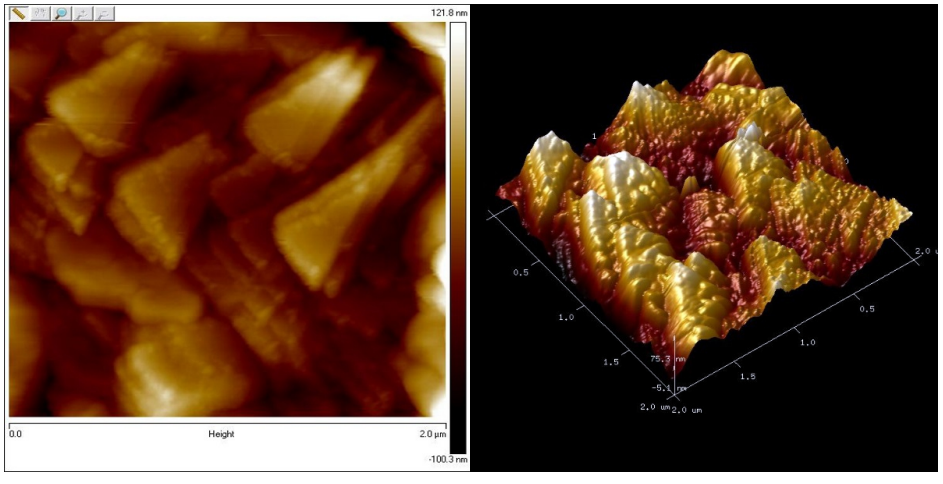

(e) (f)

Fig. 5. AFM images of $BaTiO_3$ thin films prepared at substrate temperatures of 250 to 350 °C at an interval of 50 °C.

3.5. Dielectric constant and dielectric loss as a function of frequency

The dielectric constants of the $BaTiO_3$ thin films have been measured in a frequency range of 20 Hz to 1 MHz as shown in Fig. 6. The dielectric constant decreases with an increase in frequency and attains a constant value at higher frequency, showing dispersion behaviour. The graph shows that the dielectric constant decreases with an increase in substrate temperature. Dielectric relaxations at lower frequency in perovskite ferroelectric materials represent the change in polarization according to a time-varying applied electric field. It depends upon frequency, as various mechanisms responsible for polarization are effective at different frequencies. The dielectric properties are strongly influenced by the presence of complexity of grain boundaries, grain size and orientation as well as ionic space-charge carriers. Thus, dielectric relaxations occurring at low frequency can be related to ionic space-charge carriers, such as oxygen vacancies and defects generated during the film growth [32]. The high value of dielectric constant is observed at lower frequency due to space charge polarization, indicating the inhomogeneous dielectric structure of the sample [33]. At higher frequencies the dielectric constant remains unchanged; it may be due to the inability of electric dipoles to follow up the fast variation of the applied alternating electric field. Consequently, the occurrence of friction between dipoles results in energy dissipation in the form of heat [34]. The dielectric constant is calculated by using the relation:

$$\varepsilon' = \frac{Ct}{\varepsilon_0 A} \tag{3}$$

where 'C' is capacitance, 't' is the film thickness, 'A' is an area of the film and 'ε_0' is the permittivity of free space $= 8.854 \times 10^{-12}$(F/m). The dielectric loss (tanδ) measured at room temperature is shown in Fig. 7. The graph of dielectric loss shows similar behavior as that of dielectric constant. The graph shows higher values of dielectric loss at lower frequency.

3.6. Impedance spectroscopy

Fig. 8 shows the impedance plots of $BaTiO_3$ thin films deposited at substrate temperature of 250 to 350 °C at the interval of 50 °C. An impedance spectrum also called Nyquist plot or coal-coal plot, is the plot of the imaginary (Z") versus real (Z') part of the impedance. In the present work, the only single semi-circular arc has been obtained for $BaTiO_3$ thin film. However, this semicircle is not fully displayed, the diameter may be extrapolated readily which indicates that the impedance mainly originates from the contribution of the grain interior because the grain boundary usually exhibits a much higher resistance than that of the grain interior due to the potential barrier in the grain boundary [35].

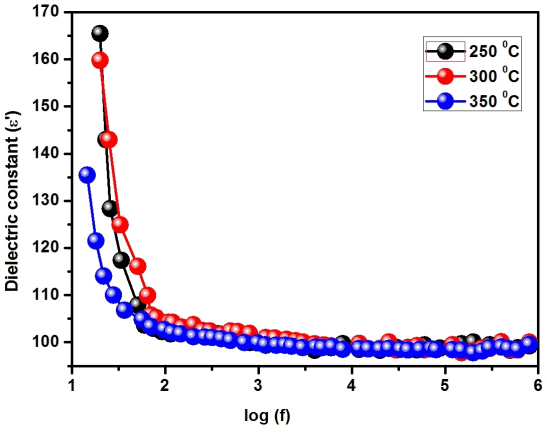

Fig. 6. Variation of dielectric constant with frequency at room temperature for $BaTiO_3$ thin films.

3.7. AC conductivity

To understand the conduction mechanism AC conductivity has been studied. Fig. 9 shows the plot of log (σ_{ac}) against log ω^2. The AC conductivity increases with an increase in frequency. As frequency of the applied field increases, hopping of carriers also increases, thereby increasing conductivity. There are two types of polarons, small polarons and large polarons. In the case of small polarons the conductivity increases linearly with an increase in the frequency. The AC conductivity can be calculated by using the following formula:

$$\sigma_{ac} = \varepsilon_0 \varepsilon' \omega^2 \tan\delta \tag{4}$$

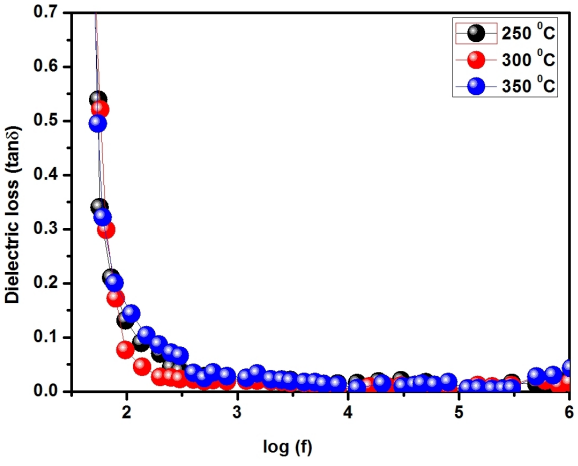

Fig. 7. Variation of dielectric loss with frequency at room temperature for $BaTiO_3$ thin films.

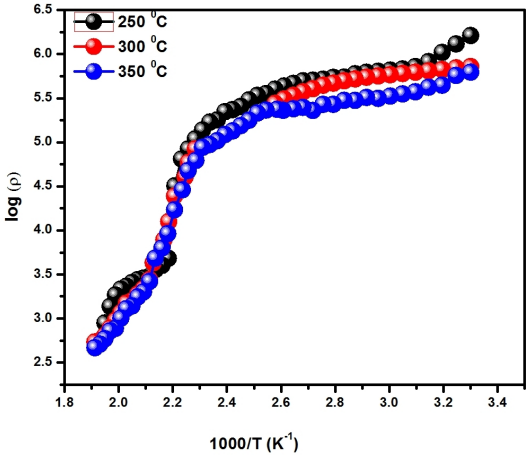

Fig. 9. Variation of DC electrical resistivity with temperature for $BaTiO_3$ thin films.

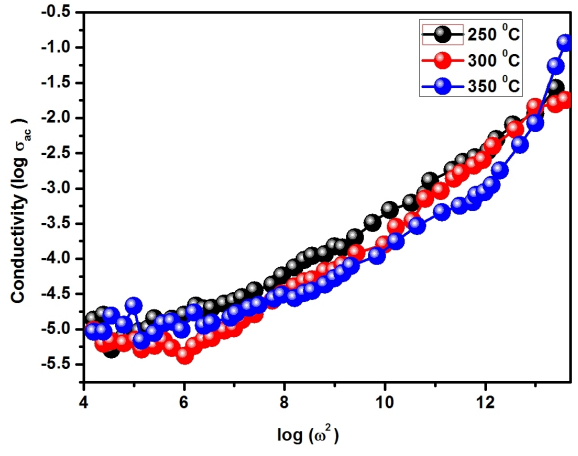

Fig. 8. Variation of AC conductivity with frequency at room temperature for $BaTiO_3$ thin films.

where ε' is the dielectric constant, ε_0 is the permittivity of free space (8.85×10^{-14} F/cm), tanδ is the loss tangent and ω is the angular frequency (i.e. $\omega = 2\pi f$) [36].

3.8. DC resistivity measurement

Fig. 10 shows the DC resistivity of $BaTiO_3$ thin films deposited at substrate temperature from 250 °C to 350 °C onto a quartz substrate. The first region observed at lower temperatures is due to impurities and may be attributed to the ordered state of ferroelectric phase and the second region of higher temperature, which is due to polaron hopping may be attributed to the disordered paraelectric state. The DC resistivity decreases with increasing temperature because with an increase in thermal energy, the electron can be released from O^{2-} ions. When an electron is introduced in the sample it may be associated with cations, which results in an unstable valence state. It is clear from the plot that the sample confirms the semiconducting behaviour, as there is a decrease in resistivity with an increase in temperature. The electrical resistivity can be explained on the basis of Verwey-de Boer mechanism in which electron exchange takes place between ions of the same element present in more than one valence state. Such ions are distributed randomly over crystallographically equivalent lattice sites [37].

3.9. PE-hysteresis loop measurement

Fig. 11 shows the hysteresis loop of $BaTiO_3$ thin films. The P-E hysteresis loops provide direct evidence for the ferroelectricity of $BaTiO_3$ thin films [38]. It can be seen that the shape of the hysteresis loops corresponds to a ferroelectric phase. When the electric field becomes sufficiently high to switch dipoles in crystallites, the polarization changes sharply and reaches saturation at higher fields. In the present case the value of saturation polarization is 0.04 μC/cm^2, which is much lower than the corresponding bulk values [39].

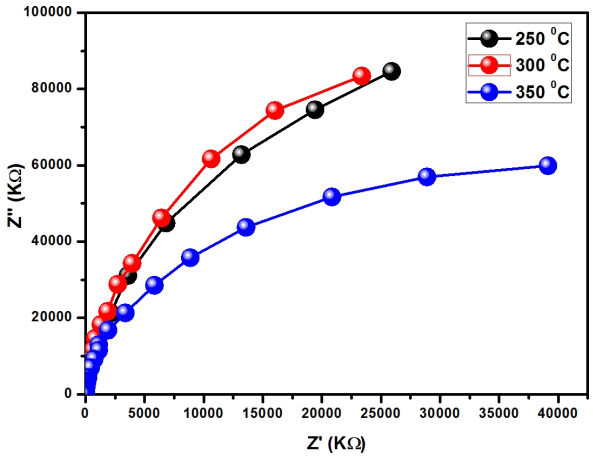

Fig. 10. Complex impedance spectra of $BaTiO_3$ thin films.

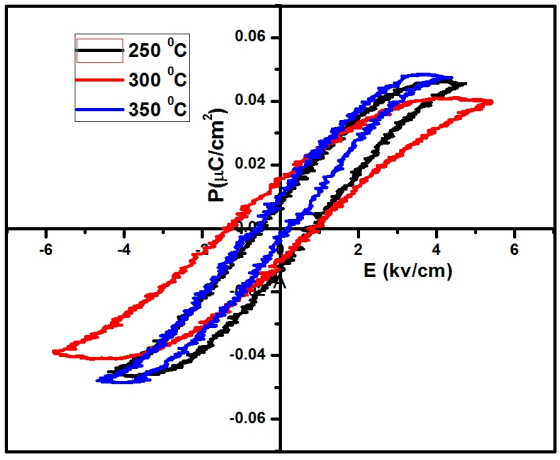

Fig. 11. PE-Hysteresis loop measurement at room temperature of $BaTiO_3$ thin films.

4. Conclusions

The ferroelectric thin films of $BaTiO_3$ were successfully prepared onto a glass substrate at various deposition temperatures from 250 °C to 350 °C at the interval of 50 °C by spray pyrolysis method. The deposited films exhibit polycrystalline nature. The phase formation has been confirmed by X-ray diffraction analysis. The SEM and AFM images show a cube-like structure of the grains, which covers the whole surface of the substrate. It is found that the grain size decreases with an increase in substrate temperature. The higher values of dielectric constant at lower frequency are due to dielectric dispersion. The electrical properties of the grains and grain boundaries have been studied by using impedance spectroscopy. To understand the conduction mechanism the AC conductivity has been studied. The measured value of saturation polarization, 0.04 $\mu C/cm^2$, is very low.

Acknowledgements

S.S. Kumbhar is very much thankful to the Department of Physics, Shivaji University, Kolhapur, for awarding the Departmental Research Fellowship (DRF) and UGC DSA-I, DST FIST-II programmes for the financial support.

References

[1] JOMNI F., GONON P., KAMEL F.E., YANGUI B., *Integr. Ferroelectr.*, 97 (2008), 121.
[2] ZHU W., WANG C.C., AKBAR S.A., ASIAIE R., *J. Mater. Sci.*, 32 (1997), 4303.
[3] KIM S., KWON O.Y., *J. Mater. Sci.*, 34 (1999), 707.
[4] WEI Z., NODA M., *Integr. Ferroelectr.*, 52 (2010), 111.
[5] LUO W.B., ZHU J., *Integr. Ferroelectr.*, 406 (2010), 56.
[6] OSUMI T., NISHIDE M., *Integr. Ferroelectr.*, 133 (2012), 42.
[7] XU T., WANG J., SHIMADA T., *J. Phys.-Condens. Mat.*, 25 (2013), 415901.
[8] HAN X.Q., KAM C.H., *Integr. Ferroelectr.*, 33 (2001), 221.
[9] SUZUKI T., NISHI Y., FUJIMOTO M., *Philos. Mag. A*, 79 (1999), 2461.
[10] PONTES F.M., PINHEIRO C.D., *J. Lumin.*, 104 (2003), 175.
[11] YOKOTA K., MORIGOU H., MIYASHITA F., *Nucl. Instrum. Meth. B*, 257 (2007), 468.
[12] MISRA M., KOTANI K., *Appl. Surf. Sci.*, 237 (2004), 421.
[13] SILVAN M.M., COBAS L.F., PALMA R.J.M., VELEZ M.H., DUART J.M.M., *Surf. Coat. Tech.*, 151 (2002), 118.
[14] HSI C.S., SHIAO F.Y., WU N.C., WANG M.C., *Solid State Commun.*, 125 (2003), 633.
[15] TAN C.K., GOH G.K.L., LAU G.K., *Thin Solid Films*, 516 (2008), 5545.
[16] KUMARI S., TRIPATHI C., SINGH A.P., CHAUHAN D., SHRIVASTAV R., DASS S., SATSANGI V.R., *Curr. Sci. India*, 91 (2006), 1062.
[17] PANDA B., DHAR A., NIGAM G.D., BHATTACHARYA D., RAY S. K., *Thin Solid Films*, 332 (1998), 46.
[18] WANG J., WAN H., LIN Q., *Mater. Sci. Tech.-Lond.*, 14 (2003), 172.
[19] JAMES A.R., PRAKASH C., PRASAD G., *J. Phys. D Appl. Phys.*, 39 (2006), 1635.
[20] QIAO L., BI X., *J. Phys. D Appl. Phys.*, 42 (2009), 1755081.
[21] GOLEGO N., STUDENIKIN S.A., COCIVERA M., *Chem. Mater.*, 10 (1998), 2000.

[22] SHINDE P.S., SADALE S.B., *Sol. Energ. Mat. Sol. C.*, 92 (2008), 283.
[23] SHINDE S.S., BHOSALE C.H., *J. Photoch. Photobio. B*, 120 (2013), 1.
[24] MAHADIK M.A., SHINDE S.S., *Mater. Res. Bull.*, 48 (2013), 4058.
[25] SAPKAL R.T., SHINDE S.S., *J. Photoch. Photobio. B*, 110 (2012), 15.
[26] ZARATE R.A., CABRERA A.L., *J. Phys. Chem. Solids*, 59 (1998), 1639.
[27] TRIPATHI A.K., CHARIAR V., GOEL T.C., PILLAI P.K.C., *Mater. Sci. Eng. B-Adv.*, 25 (1994), 34.
[28] HWANG U.Y., PARK H.S., KOO K.K., *Ind. Eng. Chem. Res.*, 43 (2004), 728.
[29] PHULE P.P., RISBUD S.H., *Mater. Sci. Eng. B-Adv.*, 3 (1989), 241.
[30] HONG H., MENG H., KUN Z., FANG T., BIN L., JUAN J., HAO C., LIANG Z., QI L., ZHEN Y., *Chinese Phys. Lett.*, 22 (2005), 2950.
[31] LV H., MA L., ZENG P., KE D., PENG T., *J. Mater. Chem.*, 20 (2010), 3665.
[32] LEE S., KANG K.Y., HAN S.K., *Appl. Phys. Let.*, 75 (1999), 1784.
[33] KANAMADI C.M., KULKARNI S.R., *Mater. Chem. Phys.*, 116 (2009), 6.
[34] BAMMANNAVAR B.K., NAIK L.R., CHOUGULE B.K., *J. Appl. Phys.*, 104 (2008), 0641231.
[35] WU J., WANG J., *J. Appl. Phys.*, 110 (2011), 064104.
[36] PATIL D.R., LOKARE S.A., *Mater. Chem. Phys.*, 104 (2007), 254.
[37] DUBEY A.K., SINGH P., SINGH S., KUMAR D., PARKASH O., *J. Alloy. Compd.*, 509 (2011), 3899.
[38] JO J.Y., KIM Y.S., KIM D.H., KIM J.D., CHANG Y.J., KONG J.H., PARK Y.D., SONG T.K., YOON J.G., JUNG J.S., NOH T.W., *Thin Solid Films*, 486 (2005), 149.
[39] VIJATOVIC M.M., BOBIC J.D., STOJANOVIC B.D., *Sci. Sinter.*, 40 (2008), 155.

Received 2015-03-07
Accepted 2015-09-07